# Z-Source Inverter-Based Approach to the Zero-Crossing Point Detection of Back EMF for Sensorless Brushless DC Motor

Changliang Xia, *Senior Member, IEEE*, and Xinmin Li

***Abstract*—Based on the Z-source inverter, this paper proposed a novel approach to zero-crossing point (ZCP) detections during the shoot-through vectors for sensorless brushless dc motor (BLDCM). The proposed approach separates the ZCP detections from speed adjustment, and makes the shoot-through vector not influence the motor speed-adjustment directly, while the zero-vectors and active-vectors are used exclusively to adjust the speed of BLDCM. With the proposed approach, the sensorless BLDCM can operate in a wide speed range without switching the detection points and the reference levels, and it is unnecessary to change the reference levels according to the PWM technique. The terminal voltages limited by diode can be directly compared with the reference zero level during the shoot-through vectors, so as to reduce the detection error caused by attenuation. Moreover, Z-source inverter not only provides boost voltage for sensorless BLDCM drive system, but also improves the utilization rate of dc source voltage and the safety of the drive system. In addition, this paper analyzed the terminal voltages of the floating phase during each vector. The experimental results verified the correctness of above theories and proved the effectiveness of the proposed approach.**

***Index Terms*—Brushless dc motor, sensorless, zero-crossing point detection, Z-source inverter.**

## I. Introduction

DUE to its compact and simple structure, reliable operation and low maintenance costs, brushless dc motor (BLDCM) has been widely used in industry [1], [2]. Typically, the rotor positions are obtained by position sensors, such as the hall sensor [3]. However, the position sensors will increase the size of BLDCM, and its installation accuracy will affect the performance of BLDCM directly. In harsh environment with high temperature, high pressure and high humidity, the position sensors are no longer appropriate [4].

Manuscript received February 12, 2014; accepted March 31, 2014. Date of publication April 15, 2014; date of current version October 15, 2014. This work was supported by the National Key Basic Research Program of China (973 Program) under Grant 2013CB035602. Recommended for publication by Associate Editor V. Staudt.

C. Xia is with the School of Electrical Engineering and Automation, Tianjin University, Tianjin 300072, China, and also with the Tianjin Key Laboratory of Advanced Technology of Electrical Engineering and Energy, Tianjin Polytechnic University, Tianjin 300387, China (e-mail: motor@tju.edu.cn).

X. Li is with the School of Electrical Engineering and Automation, Tianjin University, Tianjin 300072, China (e-mail: lixinmin@tju.edu.cn).

Color versions of one or more of the figures in this paper are available online at http://ieeexplore.ieee.org.

Digital Object Identifier 10.1109/TPEL.2014.2317708

The back EMF method is one of the most popular control way for sensorless BLDCM, the core of which is to detect the zero-crossing point (ZCP) of the back EMF [5]–[7]. A direct back EMF sensing method presented in [8] and [9] compares the terminal voltage of floating phase with the reference zero voltage during the zero vectors. The ZCP can be acquired when the compared results change relative to the previous cycle. With no use of virtual neutral point, the direct back EMF sensing method avoids the unwanted delay in [7], and the current sensors are also unnecessary. However, this method is not suitable for high-speed operation, for the pulse width of zero-vector may be very short.

Recently, the research about direct back EMF sensing method focuses on two aspects. One is to extend its application to the method to a wide range of speed and load torque, and to increase the utilization rate of dc source voltage. Another is to improve its precision.

In [10] and [11], where ZCP detections are executed during active vectors, the duty cycle of active vectors can reach 1, ensuring the utilization rate of dc source voltage, but this method is not applicable to the low-speed range with very narrow pulse width of active vectors. In [12]–[15], switching detection points according to the speed range, the ZCP detections are executed during the active vectors and the zero vectors, respectively. This method allows the BLDCM to operate within a wide speed range, and ensures the utilization rate of dc source voltage. The methods proposed in [10], [12], and [13] are all implemented by special ICs or comparator circuits. Since DSP and FPGA chips are integrated with A/D converter module, the methods implemented in [11], [14] and [15], carry out A/D sampling and ZCPs are calculated by the controller. The methods proposed in [11] and [14] are only designed for a specific kind of PWM technique. However, the method proposed in [15] is suitable for several kinds of PWM techniques by setting the corresponding reference level according to the type of PWM technique.

In order to improve the detection precision, the complementary PWM is introduced in [10], [16], and [17]. With the complementary PWM, the current freewheels through two MOSFETs on the lower arms or the higher arms, reduce the conduction losses of power devices, eliminate the detection errors introduced by antiparallel diode, and avoid the influence of discontinuous current on ZCP detections under lightly loaded conditions. But for safety concern, it is necessary to set a dead-time for the complementary PWM.

There are still several challenges for the existing methods. The first is to avoid switching detection points and reference

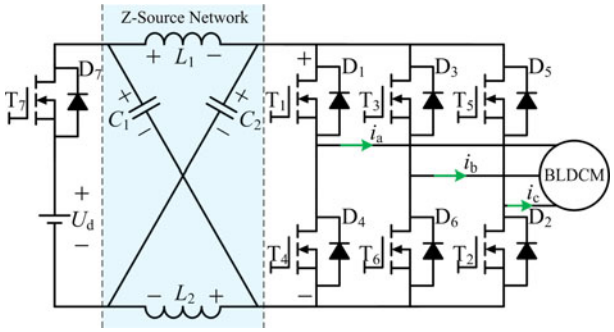


Fig. 1. Z-source inverter-based BLDCM drive system.

levels, and to carry out ZCP detections and speed adjustment separately. The second is to increase the utilization rate of dc source voltage. The last is to improve the precision.

Z-source inverter proposed in [18] allows the shoot-through vector prohibited in conventional voltage-source inverters, makes the dead-time unnecessary, and has the ability to boost voltage with the shoot-through states. It has been widely used for motor drive systems [19]. Moreover, the topological theory [20], PWM technique [21], and control method [22], [23] have been studied. Z-source inverter is also used for BLDCM speed-adjustment with its characteristic of boosting voltage in [24] and [25], but few literatures exploring its advantages to enhance the ZCP detection for sensorless BLDCM.

Z-source inverter improves the stability and safety of BLDCM drive system under complex conditions. On this basis, the paper aims to study the approach to the ZCP detection with Z-source inverter for sensorless BLDCM, which is applicable to the industrial processes supplied by low-voltage dc source, such as fuel cell, lithium battery, and photovoltaic cell, etc.

## II. Operation Principles of Z-Source Inverter-Based BLDCM Drive System

Fig. 1 shows the topology of Z-source inverter-based BLDCM drive system. It consists of the dc source $(U_{\rm d}, {\rm D}_7, {\rm T}_7)$, symmetrical Z-source network $(C_1 = C_2, L_1 = L_2)$, three-phase bridge inverter (MOSFET: ${\rm T}_1 \sim {\rm T}_6$, antiparallel diode: ${\rm D}_1 \sim {\rm D}_6$) and the BLDCM.

The diode ${\rm D}_7$ is antiparalleled with a MOSFET ${\rm T}_7$ turned ON in non-shoot-through states [26]. With this configuration, Z-source inverter can completely avoid unwanted operation modes, improve performance under lightly loaded conditions, and simplify the parameter design of Z-source network [27].

### A. Operation Principles of Z-Source Inverter

Fig. 2 shows the equivalent circuits of Z-source network in shoot-through states and non-shoot-through states.

The $u_{\rm in}$ and $i_{\rm in}$ are the output voltage and output current of Z-source network, respectively, and the reference directions of voltages and currents are all shown in Fig. 2. Due to the symmetrical Z-source network, the voltages and currents of each

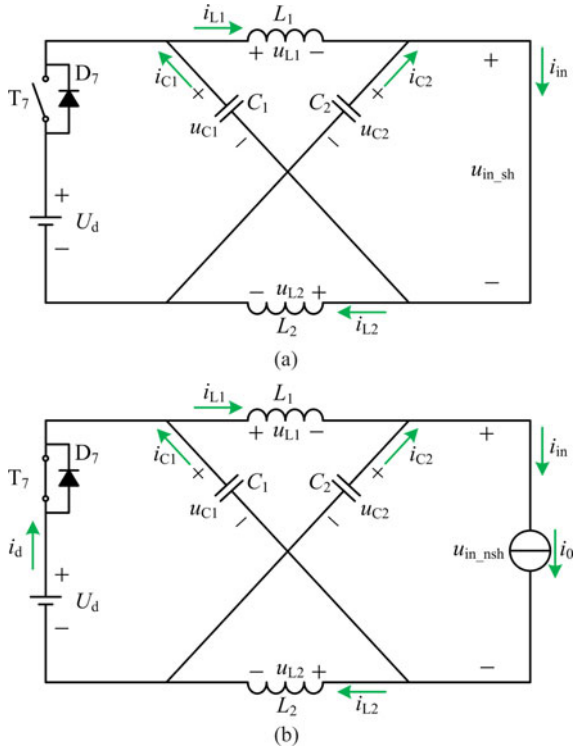


Fig. 2. Equivalent circuits of Z-source network. (a) Shoot-through state. (b) Nonshoot-through state.

part satisfy the following relationships:

$$\begin{cases} U_{\rm C1} = U_{\rm C2} = U_{\rm C} \\ u_{\rm L1} = u_{\rm L2} = u_{\rm L} \end{cases} \tag{1}$$

$$\begin{cases} I_{\rm L1} = I_{\rm L2} = I_{\rm L} \\ i_{\rm C1} = i_{\rm C2} = i_{\rm C} \end{cases} \tag{2}$$

where $U_{\rm C1}$ and $U_{\rm C2}$ are the average voltages of capacitance $C_1$ and $C_2$, respectively; $I_{\rm L1}$ and $I_{\rm L2}$ are the average currents of inductance $L_1$ and $L_2$, respectively.

As shown in Fig. 2(a), $u_{\rm in\_sh}$ indicates the output voltage of Z-source network in shoot-through states. Between these variables in Fig. 2(a), we have

$$\begin{cases} u_{\rm L} = U_{\rm C} \\ i_{\rm in} = 2I_{\rm L} \\ u_{\rm in\_sh} = 0 \ . \end{cases} \tag{3}$$

In non-shoot-through states, the output current of Z-source network can be represented by a constant current source $i_0$ by neglecting its ripple content. As shown in Fig. 2(b), $u_{\rm in\_nsh}$ indicates the output voltage of Z-source network in non-shoot-through states. Between these variables in Fig. 2(b), we have

$$\begin{cases} u_{\rm L} = U_{\rm d} - U_{\rm C} \\ i_{\rm in} = i_0 \\ u_{\rm in\_nsh} = 2U_{\rm C} - U_{\rm d} \ . \end{cases} \tag{4}$$

Within a modulation period $T_{\rm s}$, the duration of the shoot-through state and non-shoot-through state are $T_{\rm sh}$ and $T_{\rm nsh}$,

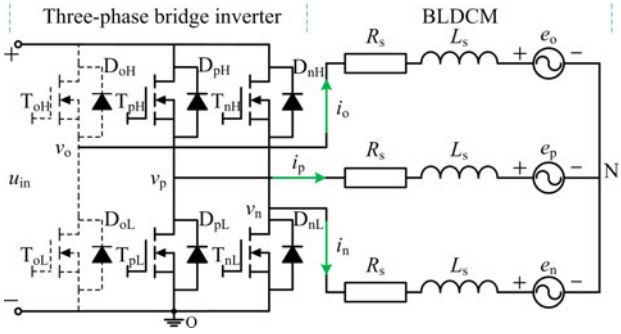


Fig. 3. Equivalent circuit of three-phase bridge inverter and BLDCM.

respectively. Average the Z-source inductor voltage $u_{\mathrm{L}}$ over a modulation period ($T_{\mathrm{sh}} + T_{\mathrm{nsh}} = T_{\mathrm{s}}$), then we have

$$U_{\mathrm{C}} T_{\mathrm{sh}} + (U_{\mathrm{d}} - U_{\mathrm{C}}) \cdot T_{\mathrm{nsh}} = 0. \tag{5}$$

By (5), the relationship between the $U_{\mathrm{C}}$ and the dc source voltage $U_{\mathrm{d}}$ is derived as

$$U_{\mathrm{C}} = \frac{1 - d_{\mathrm{s}}}{1 - 2d_{\mathrm{s}}} U_{\mathrm{d}} \tag{6}$$

where $d_{\mathrm{s}} = T_{\mathrm{sh}}/T_{\mathrm{s}}$ is the shoot-through duty cycle. By (4), the relationship between the $u_{\mathrm{in\_nsh}}$ and $U_{\mathrm{d}}$ in the non-shoot-through states can be expressed as

$$u_{\mathrm{in\_nsh}} = 2U_{\mathrm{C}} - U_{\mathrm{d}} = \frac{1}{1 - 2d_{\mathrm{s}}} U_{\mathrm{d}} = BU_{\mathrm{d}} \tag{7}$$

where $B = 1/(1 - 2d_{\mathrm{s}})$ is the boost factor. If $0 < d_{\mathrm{s}} < 0.5$, then the boost factor $B > 1$, so the shoot-through duty cycle provides the ability to boost voltage for sensorless BLDCM drive system.

### *B. PWM Technique of Z-source Inverter-Based BLDCM Drive System*

Fig. 3 shows the equivalent circuit of the three-phase bridge inverter and BLDCM. The BLDCM is connected to a three-phase bridge inverter with the six-step commutation, where only two of the three phases are conducting while the third phase called "floating phase" is unexcited. The reference directions of voltages and currents are shown in Fig. 3, where $R_{\mathrm{s}}$ and $L_{\mathrm{s}}$ denote phase resistance and phase inductance, respectively. According to the actual current direction, the current on the "positive phase" has the same direction with the reference while the current on the "negative phase" has the opposite direction with the reference. $v_{\mathrm{p}}, v_{\mathrm{n}}$, and $v_{\mathrm{o}}$ represent the terminal voltages for the "positive phase", "negative phase", and "floating phase", respectively. Similarly, $i_{\mathrm{p}}, i_{\mathrm{n}}$, and $i_{\mathrm{o}}$ indicate the phase currents of the three phases, respectively, and $e_{\mathrm{p}}, e_{\mathrm{n}}$, and $e_{\mathrm{o}}$ indicate the back EMFs of three phases, respectively. $v_{\mathrm{NO}}$ denotes the voltage of neutral point "N". $u_{\mathrm{pn}}$ represents the phase-to-phase voltage between conducting phases. The level of point "O" is the reference zero level for $v_{\mathrm{p}}, v_{\mathrm{n}}, v_{\mathrm{o}}$, and $v_{\mathrm{NO}}$.

Fig. 4 shows that the ideal back EMFs of BLDCM are trapezoidal waveform and the ideal currents of conducting phases are square waveform. $\theta$ represents the electrical angle, and the commutation cycle of each step is 60° electrical angles. As shown in Fig. 4, each edge of the curve CP represents a commutation point and each edge of the curve ZCP represents a ZCP of the back EMF. Moreover, each ZCP leads next commutation point 30° electrical angles. Therefore, by detecting the ZCP of back EMF of floating phase, and further delaying the corresponding time of 30° electrical angles, the commutation signals can be achieved.

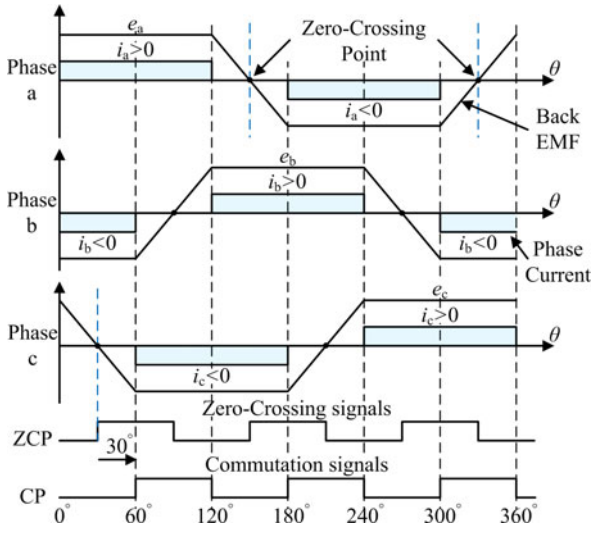


Fig. 4. Ideal back-EMFs, ideal phase currents, zero-crossing signals, and commutation signals.

The terminal voltages of three phases are shown as

$$\begin{cases} v_{\mathrm{p}} = R_{\mathrm{s}} i_{\mathrm{p}} + L_{\mathrm{s}} \frac{\mathrm{d}i_{\mathrm{p}}}{\mathrm{d}t} + e_{\mathrm{p}} + v_{\mathrm{NO}} \\ v_{\mathrm{n}} = R_{\mathrm{s}} i_{\mathrm{n}} + L_{\mathrm{s}} \frac{\mathrm{d}i_{\mathrm{n}}}{\mathrm{d}t} + e_{\mathrm{n}} + v_{\mathrm{NO}} \\ v_{\mathrm{o}} = R_{\mathrm{s}} i_{\mathrm{o}} + L_{\mathrm{s}} \frac{\mathrm{d}i_{\mathrm{o}}}{\mathrm{d}t} + e_{\mathrm{o}} + v_{\mathrm{NO}}. \end{cases} \tag{8}$$

Since $i_{\mathrm{p}} = -i_{\mathrm{n}}$ and $e_{\mathrm{p}} = -e_{\mathrm{n}}$, adding the first and the second equations of (8), the neutral point voltage can be derived as

$$v_{\mathrm{NO}} = \frac{v_{\mathrm{p}} + v_{\mathrm{n}}}{2}. \tag{9}$$

Substituting (9) into the third equation of (8), and considering $i_{\mathrm{o}} = 0$, the terminal voltage of floating phase can be written as

$$v_{\mathrm{o}} = \frac{v_{\mathrm{p}} + v_{\mathrm{n}}}{2} + e_{\mathrm{o}}. \tag{10}$$

From (10), if $v_{\mathrm{p}}$ and $v_{\mathrm{n}}$ are available, then $v_{\mathrm{o}}$ can be derived, and the ZCP of $e_{\mathrm{o}}$ will be obtained.

The conventional PWM provides active power during the active vectors, and the current freewheel through the antiparallel diode and MOSFET during the zero vectors, but the shoot-through vector is forbidden to appear. However, active vectors, zero vectors, and shoot-through vectors are all allowed for the PWM of Z-source inverter.

The vector $\boldsymbol{V}(x_3, x_2, x_1, x_0)$ is defined to indicate the switch states of the MOSFETs of the conducting phases, and bit variables $x_3, x_2, x_1, x_0$ represent the switch states of $\mathrm{T_{pH}}, \mathrm{T_{pL}}, \mathrm{T_{nH}}, \mathrm{T_{nL}}$, respectively. The state "1" means that the

TABLE I
VECTORS AND OUTPUT VOLTAGE OF Z-SOURCE INVERTER

| Vector | $u_{pn}$ | $T_{pH}$ | $T_{pL}$ | $T_{nH}$ | $T_{nL}$ |
|---|---|---|---|---|---|
| $V(1111)$ | 0 | 1 | 1 | 1 | 1 |
| $V(1001)$ | $u_{in}$ | 1 | 0 | 0 | 1 |
| $V(0001)$ | 0 | 0 | 0 | 0 | 1 |
| $V(0101)$ | 0 | 0 | 1 | 0 | 1 |
| $V(1000)$ | 0 | 1 | 0 | 0 | 0 |
| $V(1010)$ | 0 | 1 | 0 | 1 | 0 |

(1 = turn-ON, 0 = turn-OFF).

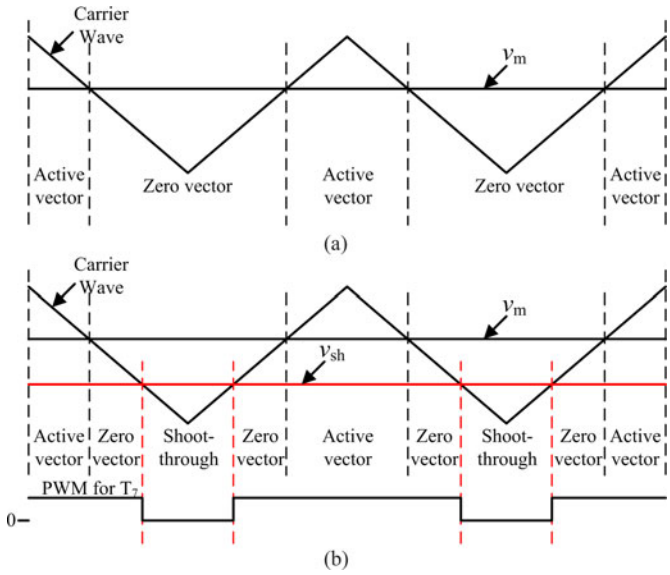


Fig. 5. PWM technique for BLDCM (a) Conventional PWM. (b) PWM of Z-Source inverter.

MOSFET is turned ON, and "0" means that the MOSFET is turned OFF.

Table I lists the vectors and their corresponding $u_{pn}$. In order to keep the MOSFETs of floating phase OFF and balance the shoot-through current, the shoot-through vector $\boldsymbol{V}(1\ 1\ 1\ 1)$ is produced by simultaneously switching on four MOSFETs of conducting phases, and $u_{pn}$ is 0 V during the shoot-through vector $\boldsymbol{V}(1\ 1\ 1\ 1)$. Similarly, the active vector $\boldsymbol{V}(1\ 0\ 0\ 1)$ is produced by switching on the MOSFETs $T_{pH}$ and $T_{nL}$, and the $u_{pn}$ equals to $u_{in}$ during the active vector $\boldsymbol{V}(1\ 0\ 0\ 1)$.

Different PWM techniques for BLDCM usually use different zero vectors. The vectors $\boldsymbol{V}(0\ 0\ 0\ 1)$, $\boldsymbol{V}(0\ 1\ 0\ 1)$, $\boldsymbol{V}(1\ 0\ 0\ 0)$, and $\boldsymbol{V}(1\ 0\ 1\ 0)$ are all zero vectors, and $u_{pn}$ of these zero vectors are all 0 V. However, the freewheeling routes among these zero vectors are different.

As shown in Fig. 5(a), the conventional PWM is implemented by the modulation level $v_m$ and carrier waves. But, as shown in Fig. 5(b), another modulation level $v_{sh}$ is utilized to produce the shoot-through vector for Z-source inverter based on the conventional PWM.

Compared with the conventional PWM, the active vectors remain unchanged for the PWM of Z-source inverter, and a part of the zero vector is replaced by the shoot-through vector. The last curve in Fig. 5(b) shows the PWM signals for $T_7$, which is OFF during the shoot-through vectors and ON during the non-shoot-through vectors.

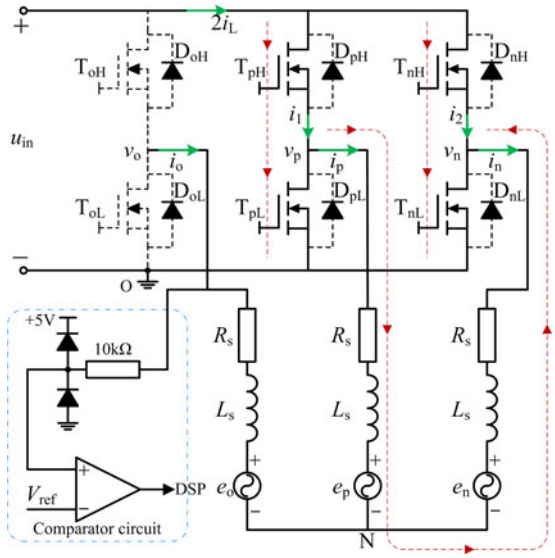


Fig. 6. Equivalent circuit during the shoot-through vector $\boldsymbol{V}(1\ 1\ 1\ 1)$.

## III. TERMINAL VOLTAGE OF FLOATING PHASE

The terminal voltage $v_p$ and $v_n$ are different during various vectors. As shown in Fig. 6, the MOSFETs $T_{pH}$, $T_{pL}$, $T_{nH}$, and $T_{nL}$ are turned ON during the shoot-through vector $V(1\ 1\ 1\ 1)$.

$R_{DS}$ denotes the on-resistance of MOSFET, and $u_D$ represents the forward voltage of antiparallel diodes. The currents flowing through the MOSFET $T_{pH}$ and $T_{nH}$ are $i_1$ and $i_2$, respectively. $v_p$ and $v_n$ during the shoot-through vectors can be written as

$$\begin{cases} v_p = (i_1 - i_p)R_{DS} \\ v_n = (i_2 - i_n)R_{DS}. \end{cases} \tag{11}$$

Substituting (11) into (10), and considering $i_p = -i_n$, the output current of Z-source network during the shoot-through vectors is $i_{in} = 2i_L = i_1 + i_2$, then $v_o$ can be derived as

$$v_o = i_L R_{DS} + e_o. \tag{12}$$

Since $R_{DS}$ is very small, the term $i_L R_{DS}$ in (12) can be neglected, and the (12) can be rewritten as

$$v_o = e_o. \tag{13}$$

From (13), with the comparator circuit shown in Fig. 6, comparing $v_o$ with zero reference level during the shoot-through vector $\boldsymbol{V}(1\ 1\ 1\ 1)$, the ZCPs of $e_o$ can be obtained.

As shown in Fig. 7, the MOSFETs $T_{pH}$ and $T_{nL}$ are turned ON during the active vector $\boldsymbol{V}(1\ 0\ 0\ 1)$.

$v_p$ and $v_n$ during the active vectors can be written as

$$\begin{cases} v_p = u_{in} - i_p R_{DS} \\ v_n = -i_n R_{DS}. \end{cases} \tag{14}$$

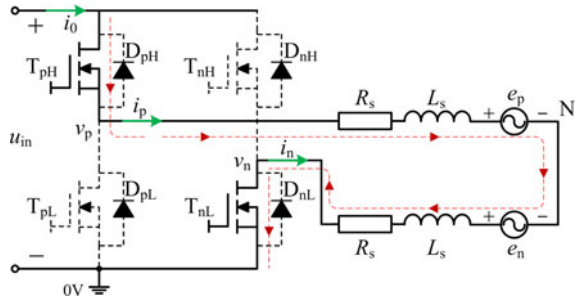


Fig. 7. Equivalent circuit during the active vector $\boldsymbol{V}(1\ 0\ 0\ 1)$.

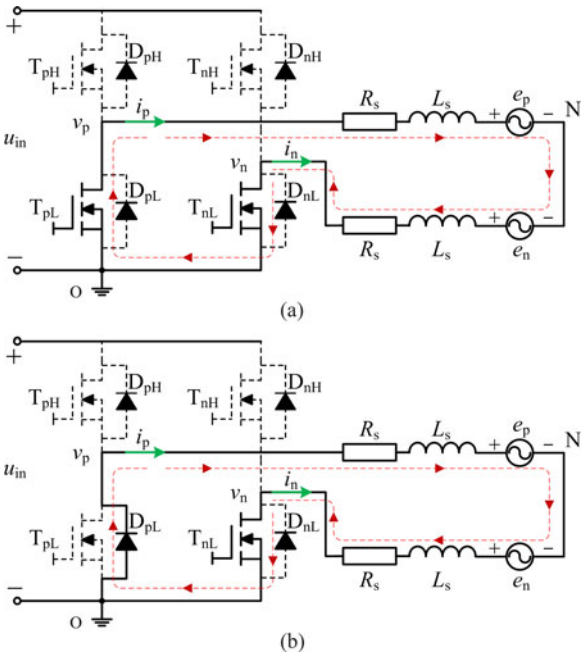


Fig. 8. Equivalent circuit during the zero vector $\boldsymbol{V}(0\ 1\ 0\ 1)$ or $\boldsymbol{V}(0\ 0\ 0\ 1)$, (a) Zero vector is $\boldsymbol{V}(0\ 1\ 0\ 1)$, (b) Zero vector is $\boldsymbol{V}(0\ 0\ 0\ 1)$.

Substituting (14) into (10), $v_o$ can be derived as

$$v_o = \frac{u_{in}}{2} + e_o. \tag{15}$$

From (15), comparing $v_o$ with the midpoint level of dc source $u_{in}/2$ during the active vector $\boldsymbol{V}(1\ 0\ 0\ 1)$, the ZCPs of $e_o$ can be obtained.

As shown in Fig. 8(a), the MOSFETs $T_{pL}$ and $T_{nL}$ are turned ON with the zero vector $\boldsymbol{V}(0\ 1\ 0\ 1)$. However, $T_{nL}$ and $D_{pL}$ are turned ON with the zero vector $\boldsymbol{V}(0\ 0\ 0\ 1)$ as shown in Fig. 8(b).

With the zero vector $\boldsymbol{V}(0\ 1\ 0\ 1)$, two MOSFETs of the conducting phases on the lower arms are utilized to freewheel the current. $v_p$ and $v_n$ during zero vector $\boldsymbol{V}(0\ 1\ 0\ 1)$ can be written as

$$\begin{cases} v_p = -i_p R_{DS} \\ v_n = -i_n R_{DS}. \end{cases} \tag{16}$$

Substituting (16) into (10), $v_o$ can be derived as

$$v_o = e_o. \tag{17}$$

With the zero vector $\boldsymbol{V}(0\ 0\ 0\ 1)$, $T_{nL}$ and $D_{pL}$ are utilized to freewheel the current. $v_p$ and $v_n$ during the zero vector

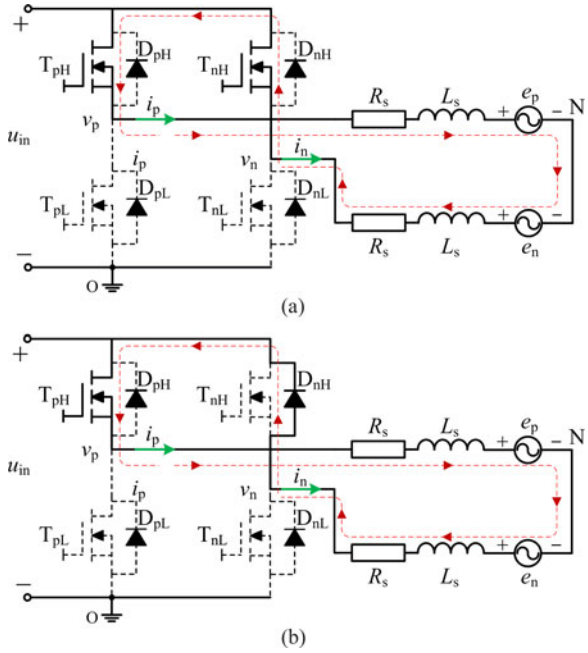


Fig. 9. Equivalent circuit during the zero vector $\boldsymbol{V}(1\ 0\ 1\ 0)$ or $\boldsymbol{V}(1\ 0\ 0\ 0)$. (a) Zero vector is $\boldsymbol{V}(1\ 0\ 1\ 0)$, (b) Zero vector is $\boldsymbol{V}(1\ 0\ 0\ 0)$.

$\boldsymbol{V}(0\ 0\ 0\ 1)$ can be written as

$$\begin{cases} v_p = -u_D \\ v_n = -i_n R_{DS}. \end{cases} \tag{18}$$

Substituting (18) into (10), $v_o$ can be derived as

$$v_o = -\frac{i_n R_{DS} + u_D}{2} + e_o. \tag{19}$$

By (17) and (19), since the term $i_n R_{DS}$ and $u_D$ can be neglected in (19), the ZCPs of $e_o$ can be obtained by comparing $v_o$ with zero reference level during the zero vector ***V(0 1 0 1)*** or $\boldsymbol{V}(0\ 0\ 0\ 1)$.

As shown in Fig. 9(a), The MOSFETs $T_{pH}$ and $T_{nH}$ are turned ON with the zero vector $\boldsymbol{V}(1\ 0\ 1\ 0)$. However, $T_{pH}$ and $D_{nH}$ are turned ON with the zero vector $\boldsymbol{V}(1\ 0\ 0\ 0)$ as shown by Fig. 9(b).

The derivation process is similar to that from (14) to (19), and $v_o$ during the zero vector $\boldsymbol{V}(1\ 0\ 1\ 0)$ can be written as

$$v_o = u_{in} + e_o. \tag{20}$$

$v_o$ during the zero vector $\boldsymbol{V}(1\ 0\ 0\ 0)$ can be written as

$$v_o = -\frac{i_p R_{DS} - u_D}{2} + u_{in} + e_o. \tag{21}$$

By (20) and (21), since the term $i_p R_{DS}$ and $u_D$ can be neglected, the ZCPs of $e_o$ can be obtained by comparing $v_o$ with the reference level $u_{in}$ during the zero vector $\boldsymbol{V}(1\ 0\ 1\ 0)$ or $\boldsymbol{V}(1\ 0\ 0\ 0)$.

In conclusion, the vectors and corresponding terminal voltages are listed in Table II.

For the zero vectors $\boldsymbol{V}(0\ 0\ 0\ 1)$ and $\boldsymbol{V}(1\ 0\ 0\ 0)$, there is an antiparallel diode that participates in the process of freewheeling, and if $e_o$ is small, the influence on the ZCP detections

TABLE II
VECTORS AND TERMINAL VOLTAGES OF THREE PHASES

| Vector | Terminal Voltage / V | | |
|---|---|---|---|
| | Positive phase | Negative phase | Floating phase |
| $\boldsymbol{V}(1111)$ | $(i_1\text{-}i_p)R_{DS}$ | $(i_2\text{-}i_n)R_{DS}$ | $i_LR_{DS}+e_o$ |
| $\boldsymbol{V}(1001)$ | $u_{in}\text{-}i_pR_{DS}$ | $-i_nR_{DS}$ | $u_{in}/2+e_o$ |
| $\boldsymbol{V}(0101)$ | $-i_pR_{DS}$ | $-i_nR_{DS}$ | $e_o$ |
| $\boldsymbol{V}(0001)$ | $-u_D$ | $-i_nR_{DS}$ | $-(i_nR_{DS}+u_D)/2+e_o$ |
| $\boldsymbol{V}(1010)$ | $u_{in}\text{-}i_pR_{DS}$ | $u_{in}\text{-}i_nR_{DS}$ | $u_{in}+e_o$ |
| $\boldsymbol{V}(1000)$ | $u_{in}\text{-}i_pR_{DS}$ | $u_{in}+u_D$ | $-(i_pR_{DS}\text{-}u_D)/2+u_{in}+e_o$ |

caused by $u_D$ should be considered. However, for the zero vectors $\boldsymbol{V}(0\ 1\ 0\ 1)$ and $\boldsymbol{V}(1\ 0\ 1\ 0)$, the freewheeling route does not contain the antiparallel diode, and the setting of dead-time is unnecessary for the Z-source inverter.

For the drive system, in order to extend the speed range and increase the voltage utilization rate of dc source, it is necessary to reduce the use of the four zero vectors whose $u_{pn}$ is 0 V. Just based on this reason, we should try to avoid detecting the ZCPs during the zero vectors for high-speed operation.

For the active vector $\boldsymbol{V}(1\ 0\ 0\ 1)$ and zero vectors $\boldsymbol{V}(1\ 0\ 1\ 0)$ and $\boldsymbol{V}(1\ 0\ 0\ 0)$, from (15), (20), and (21), it is easy to find the voltage component $u_{in}$ in these expressions. Limited by the input restriction of comparator chip and A/D sample module, $v_o$ and reference levels should be attenuated before inputting to the comparator circuit shown in Fig. 6. But the back EMF component $e_o$ is also attenuated. Just based on this reason, we should try to avoid detecting the ZCP during vectors $\boldsymbol{V}(1\ 0\ 0\ 1)$, $\boldsymbol{V}(1\ 0\ 1\ 0)$, and $\boldsymbol{V}(1\ 0\ 0\ 0)$ to reduce the detection error.

With the shoot-through vector $\boldsymbol{V}(1\ 1\ 1\ 1)$, though the voltage $u_{pn}$ is 0 V, the shoot-through vector is a boosted vector for the Z-source inverter-based BLDCM drive system, so the existence of shoot-through vector would not influence the utilization rate of dc source voltage. In addition, from (12), the voltage component $u_{in}$ and $u_D$ are not contained in the expression of $v_o$. By limiting the terminal voltages with diodes, the ZCPs of floating phase can be obtained by the comparator circuits during the shoot-through vectors.

## IV. PROPOSED APPROACH TO ZERO-CROSSING POINT DETECTION OF BACK EMF

The shoot-through vector introduced by the Z-source inverter provides a new window for detecting the ZCP of back EMF of floating phase. The six-step commutation method shown in Fig. 4 is used to drive the BLDCM. In each modulation period $T_s$, the terminal voltage of floating phase is compared with zero reference level during the shoot-through vector $\boldsymbol{V}(1\ 1\ 1\ 1)$. The detection point is fixed at the end of each shoot-through vector, and never switched at any speed range. The ZCP will be acquired when the compared results change relative to the previous cycle. Then, start a timer to delay the corresponding time of $30^\circ$ electrical angles, and the commutation signals can be achieved. In addition, the shoot-through vector will increase the dc source voltage to meet the requirement of BLDCM rated voltage. Moreover, with the proposed approach, the motor speed-adjustment will be achieved by adjusting the active vector duty cycle $d_1$. The schematic of the proposed approach for sensorless BLDCM is shown in Fig. 10.

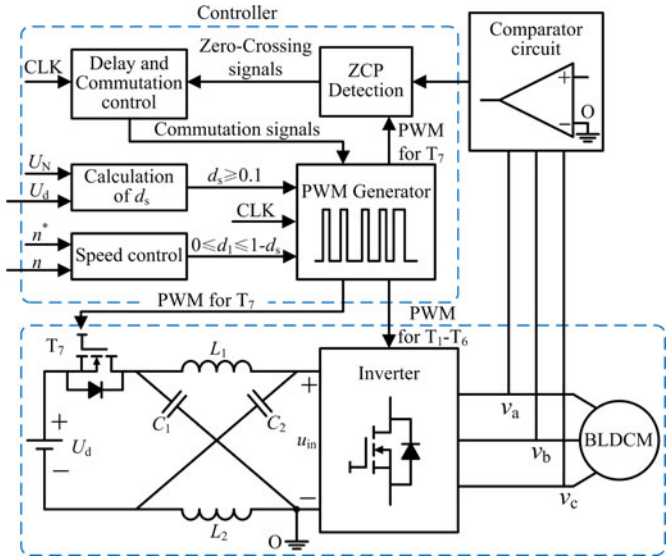


Fig. 10. Schematic of the proposed approach for sensorless BLDCM.

By (7), the average value of $u_{pn}$ can be derived as

$$U_{av} = d_1 u_{in\_nsh} = \frac{d_1}{1-2d_s}U_d \tag{22}$$

where $d_1$ is the active vector duty cycle and $U_{av}$ is the average value of $u_{pn}$. The constraint relationship between $d_1$ and $d_s$ is $0 \le d_1 \le 1-d_s$. By (22), for a given $d_s$, the $U_{av}$ gets the maximum value without any zero vector, namely $d_1 = 1-d_s$. The maximum value $U_{max}$ can be expressed by

$$U_{max} = \frac{1-d_s}{1-2d_s}U_d. \tag{23}$$

By (6) and (23), $U_{max}$ and $U_C$ have the same expression, namely $U_{max} = U_C$. Therefore, $U_{max}$ can be obtained by measuring the capacitor voltage $U_C$.

The requirement of BLDCM rated voltage $U_N$ can be satisfied when $U_{max} \ge U_N$, and the minimum $d_s$ should be ensured to enable the normal ZCP detections. If $T_s = 100\,\mu$s, under the experimental condition in this paper, it is necessary to continue the shoot-through vector for 10 $\mu$s at least, namely $d_s \ge 0.1$, for the accurate detection. $d_s$ can be set offline according to the demands.

When $U_d < U_N$, substituting $U_{max} = U_N$ into (23), the minimum shoot-through duty cycle $d_{s\_min}$ satisfying the requirement of $U_N$, can be calculated as

$$d_{s\_min} = \frac{U_N - U_d}{2U_N - U_d}. \tag{24}$$

When $U_d > U_N$ or $d_{s\_min} < 0.1$, to ensure the normal ZCP detections, the shoot-through duty cycle should be at least set as

$$d_s = 0.1. \tag{25}$$

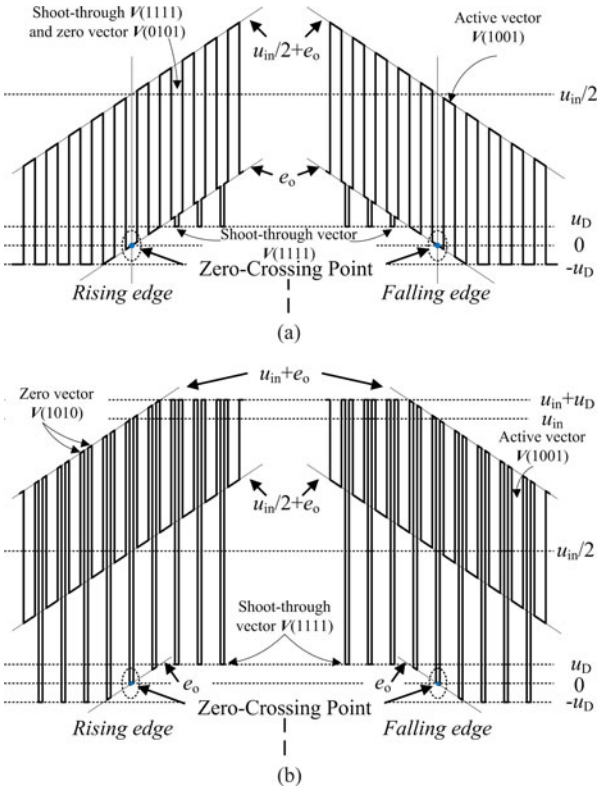


Fig. 11. Rising edge and falling edge of the terminal voltage of floating phase. (a) Zero vector is $\boldsymbol{V}(0\ 1\ 0\ 1)$. (b) Zero vector is $\boldsymbol{V}(1\ 0\ 1\ 0)$.

In conclusion, the calculation method of $d_s$ can be summarized as

$$d_s = \begin{cases} d_{s\_min}\ , & U_N \geq U_d \text{ and } d_{s\_min} \geq 0.1 \\ 0.1\ , & U_N < U_d \text{ or } d_{s\_min} < 0.1 \end{cases} \tag{26}$$

$d_1$ can be calculated offline or controlled by the reference speed $n^*$ and the actual speed $n$. With the zero vector $\boldsymbol{V}(0\ 1\ 0\ 1)$, the rising edge and falling edge of $v_o$ are shown in Fig. 11(a). As shown in Fig. 11(b), the zero vector is changed to $\boldsymbol{V}(1\ 0\ 1\ 0)$.

For Fig. 11, it is worthwhile to note that the antiparallel diode $D_{oH}$ of floating phase will be turned ON with $e_o > u_D$ during the shoot-through vectors, so it is easy to find that $v_o = u_D > 0$ in Fig.11. Similarly, the antiparallel diode $D_{oL}$ of floating phase will be turned ON with $e_o < -u_D$ during the shoot-through vectors, so it is easy to find that $v_o = -u_D < 0$. As shown in Fig. 11, this phenomenon does not affect the ZCP detections. In addition, the ZCP detection should be executed after the commutation process. If the duration of freewheeling current in floating phase is more than the corresponding time of $30^\circ$ electrical angles in special case, the ZCP detection will be influenced by the freewheeling current, and the acceleration of commutation process is necessary.

For the proposed approach, the ZCP detection is executed during the shoot-through vector, and is independent of the zero and active vectors, so it is unnecessary to set different reference levels for various PWM techniques. Moreover, the shoot-through vector does not influence the motor speed-adjustment directly, so it is also unnecessary to switch the detection points and reference levels according to the speed range.

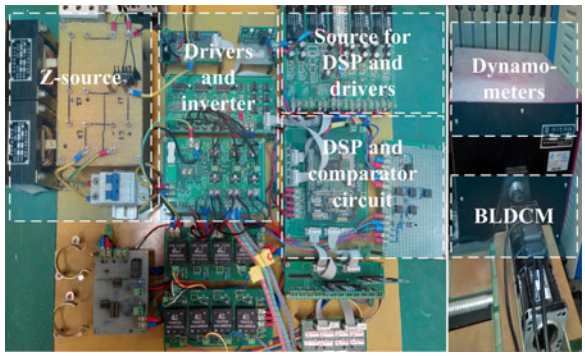


Fig. 12. Experiment prototype.

TABLE III
PARAMETERS OF BLDCM AND Z-SOURCE INVERTER

| Parameters | Value |
|---|---|
| Rated voltage $U_N$ | 24 V |
| Rated power $P_N$ | 70 W |
| Rated current $I_N$ | 4 A |
| Rated load $T_N$ | 0.23 N·m |
| Rated speed $n_N$ | 3000 r/min |
| Pairs of poles $p$ | 5 |
| Z-Source inductance $L_1$=$L_2$ | 1.5 mH |
| Z-Source capacitance $C_1$=$C_2$ | 470 μF |
| PWM frequency | 10kHz |

## V. IMPLEMENTATION AND EXPERIMENTAL RESULTS

As shown in Fig. 12, the experimental prototype is built to verify the correctness of theories and the effectiveness of the proposed approach.

In the prototype where the controller is TMS320F28335 produced by TI Company, the clock frequency is 150 MHz, and the MOSFET is IRFB7430PBF. As shown in Fig. 6, the comparator circuits are implemented by three independent comparator chips LM393A. The basic parameters of the BLDCM and Z-source inverter are listed in Table III.

The experimental prototype is supplied by an Agilent N5767A dc source. The experimental results are recorded by a digital oscilloscope DLM2024, with a logic probe PBL100 to acquire the PWM signals, zero-crossing signals, commutation signals, and hall signals. The load of the BLDCM is provided by a dynamometer which can display the speed of BLDCM in real time.

The proposed approach does not use any position sensors and current sensors. But in order to validate the proposed method, the phase current $i_a$ is measured by a current sensor and hall signals HA, HB, HC are outputted by hall sensors. When the motor is stationary or in a very low speed, the back EMFs are too small to be detected, so it is necessary to accelerate the motor by

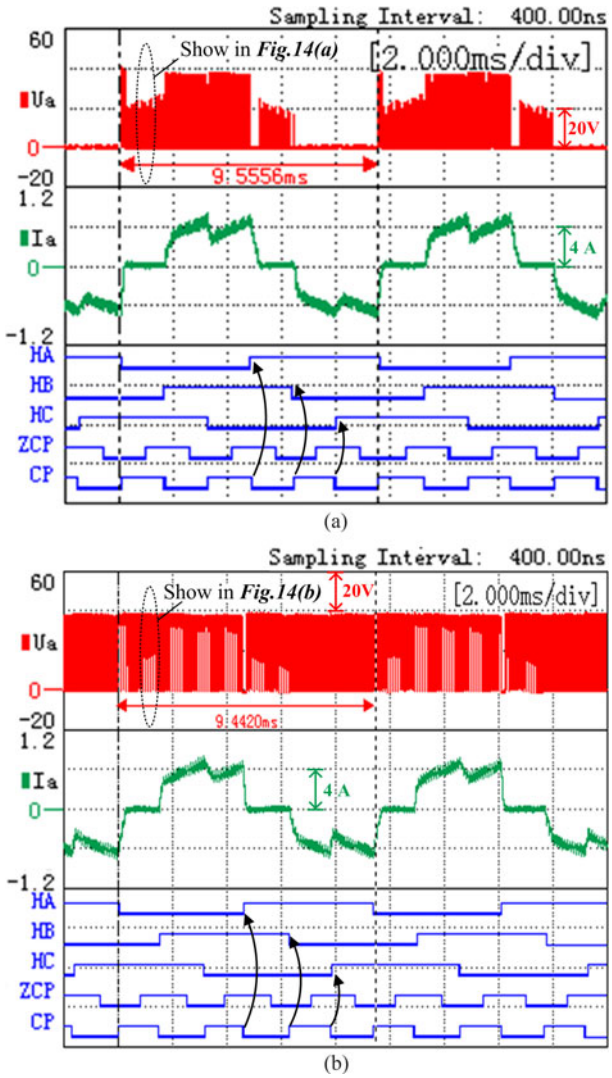


Fig. 13. Experimental result with different types of zero vectors. (a) Zero vector is $\boldsymbol{V}(0\ 1\ 0\ 1)$. (b) Zero vector is $\boldsymbol{V}(1\ 0\ 1\ 0)$.

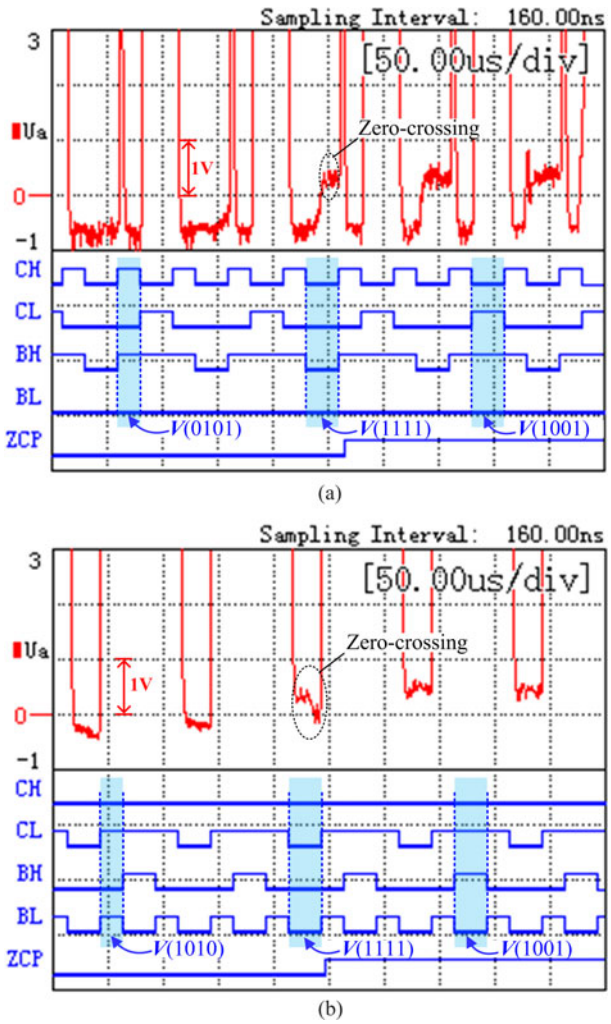


Fig. 14. Details of terminal voltage of phase "a" around the ZCP with different types of zero vectors. (a) Zero vector is $\boldsymbol{V}(0\ 1\ 0\ 1)$, (b) Zero vector is $\boldsymbol{V}(1\ 0\ 1\ 0)$.

an open-loop start method illustrated in [28]. The corresponding time of $30^{\circ}$ electrical angles can be calculated by the interval time of latest two ZCPs, and this method is illustrated in detail in [29].

The PWM used in the experiment has been shown in Fig. 5(b). Set $U_{\mathrm{d}} = 17\,\mathrm{V}, d_{\mathrm{s}} = 0.3, d_1 = 0.3$, and the load torque $T_{\mathrm{L}} = 0.23\mathrm{N}\cdot\mathrm{m}$. With the zero vector $\boldsymbol{V}(0\ 1\ 0\ 1)$ and $\boldsymbol{V}(1\ 0\ 1\ 0)$, the experimental results are shown in Fig. 13(a) and (b), respectively.

As shown in Fig. 13, each figure from top to bottom is the terminal voltage of phase "a", phase current of phase "a", three hall signals HA, HB, HC, the zero-crossing signals ZCP, and commutation signals CP. The motor speeds displayed by the dynamometer are all 1250 r/min. From Fig. 13, it can be found that the approach guarantees precise correspondence between commutation signals and hall signals, and that stable operation can be obtained. In addition, the details of terminal voltage of phase "a" around the ZCP are shown in Fig. 14.

As shown in Fig. 14, each figure from top to bottom is the terminal voltage of phase "a", PWM signals of phase "c" (CH, CL), PWM signals of phase "b"(BH, BL), and the zero-crossing signal(ZCP). The phase "a" is the floating phase at this commutation step, and the PWM signals are all active low. From Fig. 14, it can be found that there is no dead zone between zero and active vectors, and that the ZCP of floating phase can be detected correctly with different types of zero vectors.

According to Figs. 13 and 14, with different types of zero vectors, though the waveforms of terminal voltages of the floating phase are different, the commutation signals always have the same effect with the hall signals. Hence, the proposed approach is not influenced by the types of zero vectors, and is available for several kinds of PWM techniques.

The proposed approach adjusts the motor speed by changing the active vector duty cycle. In order to test the performance of the proposed approach with different speeds, set $U_{\mathrm{d}} = 17\,\mathrm{V}, d_{\mathrm{s}} = 0.3$, and $T_{\mathrm{L}} = 0.23\mathrm{N}\cdot\mathrm{m}$. Under the rated load condition, $d_1$ is set as 0.7, 0.5, and 0.1, respectively, and the experimental results are shown in Fig. 15.

As shown in Figs. 13 and 15, with the increase of the active vector duty cycle, the motor speed also increases. When $d_1 = 0.7$, the motor speed reaches to the rated speed, and the

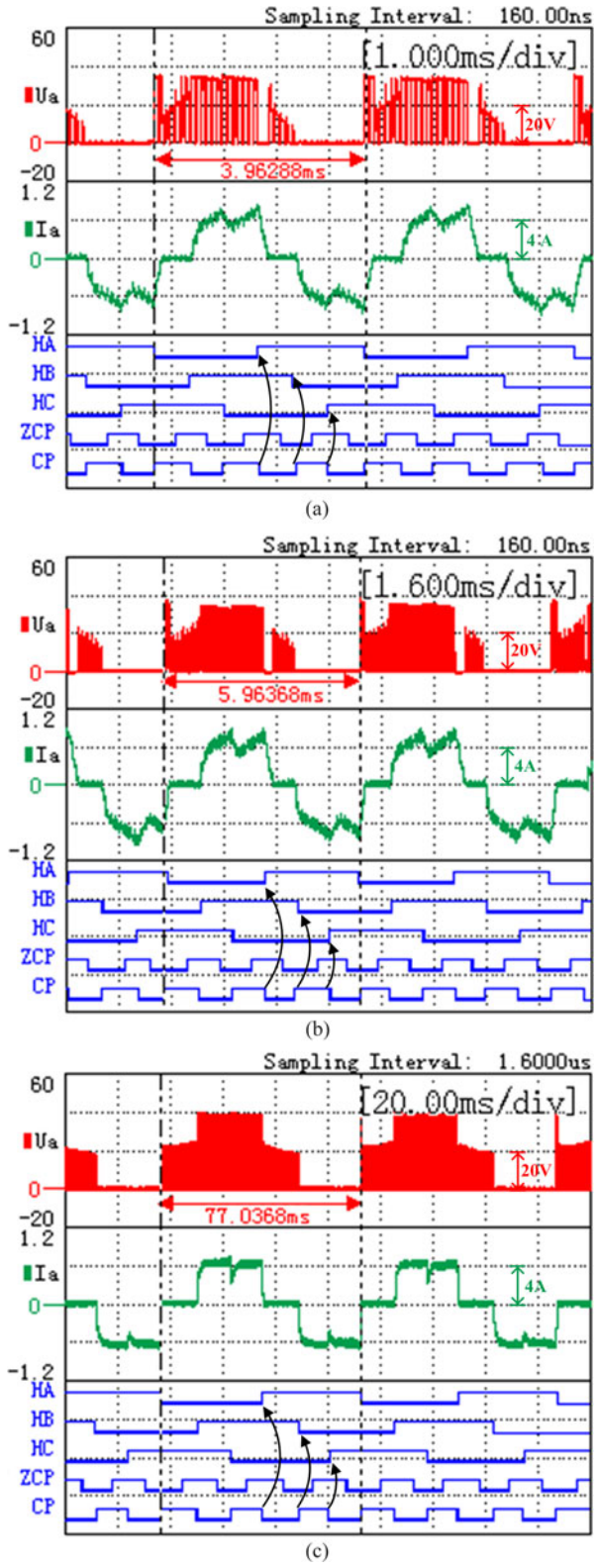


Fig. 15. Experimental results with different active vector duty cycle, (a) $d_1 = 0.7$, $n = 3000\,\mathrm{r/min}$, (b) $d_1 = 0.5$, $n = 2000\,r/\mathrm{min}$, (c) $d_1 = 0.1$, $n = 150\,\mathrm{r/min}$.

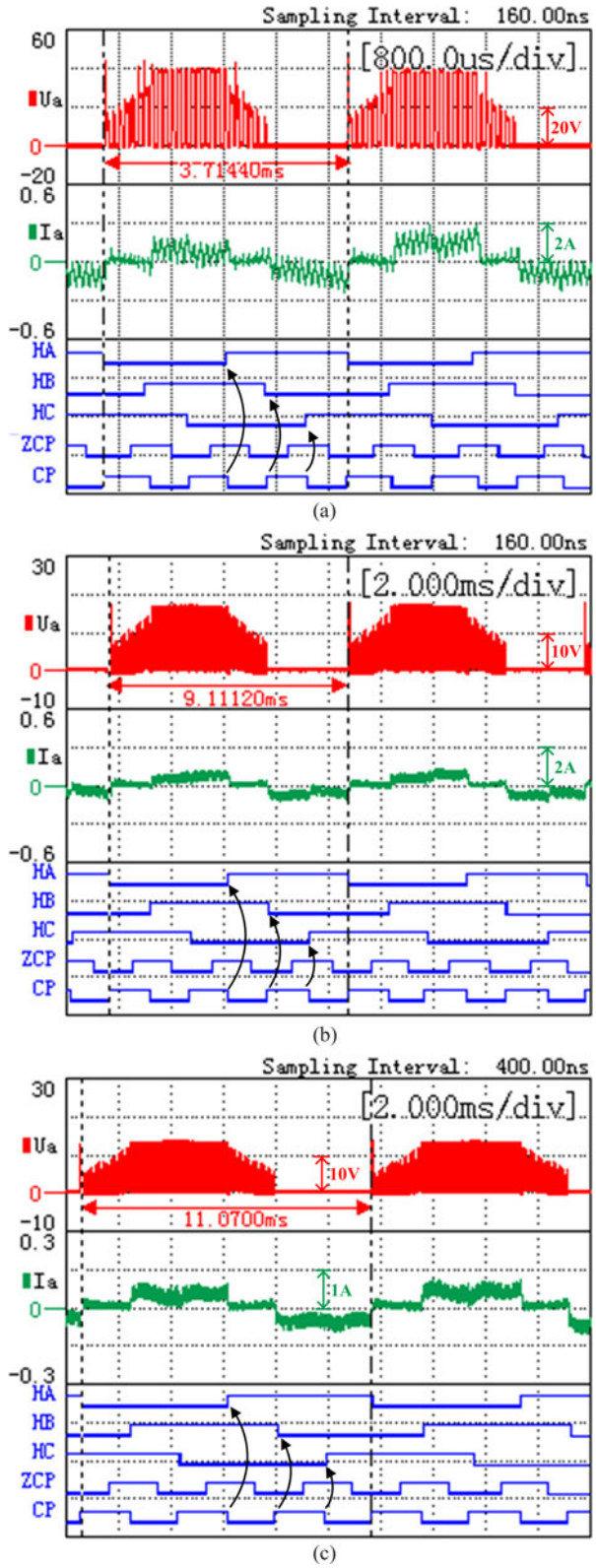


Fig. 16. Experimental result with different shoot-through vector duty cycle. (a) $d_s = 0.4$, $n = 3250\,\mathrm{r/min}$, (b) $d_s = 0.2$, $n = 1300\,\mathrm{r/min}$, (c) $d_s = 0.1$, $n = 1100\,\mathrm{r/min}$.

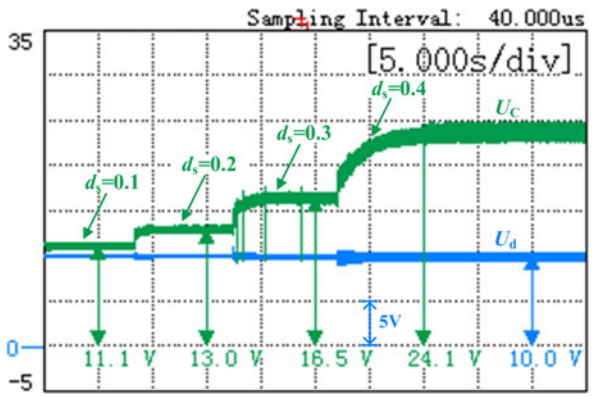


Fig. 17. DC source voltage and the capacitor voltage of Z-source inverter.

zero vector does not exist within a modulation period. However, when $d_1 = 0.1$, the motor operates at a very low speed of about 150 r/min. From another perspective, without switching the detection points and the reference levels, the BLDCM can operate within a wide speed range under the rated load condition, and the dc source voltage can be lower than the rated voltage of BLDCM, in other words, the dc source voltage can be fully used. It is easy to find that the duration of freewheeling current in floating phase is about 200 $\mu$s in Fig. 15(a), so the commutation process does not influence the ZCP detection under the rated condition. If the motor speed reaches to 5000 r/min, the corresponding time of 30° electrical angles is about 200 $\mu$s, and the ZCP detection may be affected under this special condition.

In order to test the performance of the proposed approach with different $d_s$, set $U_d = 10\,\mathrm{V}, d_1 = 0.3$, and $T_L = 0.02\mathrm{N}\cdot\mathrm{m}$. Under the lightly loaded condition, $d_s$ is set as 0.4, 0.2, and 0.1 respectively, and the experimental results are shown in Fig. 16.

As shown in Fig. 16, with different $d_s$, the proposed approach can get the zero-crossing points and the commutation points accurately, and it is also suitable for the lightly loaded condition.

For a given $d_1 = 0.5, d_s$ steps by an increment of 0.1 from 0.1 to 0.4, then the motor speed also increases. The motor can operate stably in accelerating state when the $d_s$ steps to another value. The waveforms of $U_d$ and $U_C$ are shown in Fig. 17.

For a constant $U_d, U_C$ is larger than $U_d$ with different $d_s$. Since $U_{max} = U_C$, the experimental results illustrate that $U_{max}$ is also larger than $U_d$. To be noted, because of the influence of parasitic parameters, the experimental results above may be slightly less than the theoretical values [20].

## VI. Conclusion

In this paper, the Z-source inverter-based approach to the ZCP detection is proposed for sensorless BLDCM. The proposed approach detects the ZCPs during the shoot-through vectors, and uses the zero-vectors and active-vectors to adjust the speed of BLDCM, separating ZCP detections and speed adjustment. This paper illustrates the topology and PWM technique of Z-source inverter, analyzes the terminal voltages of the floating phase during each vector. At last, a 70-W experimental prototype is built, and the experimental results verify the correctness of theories and the effectiveness of the proposed approach.

In conclusion, the proposed approach has the following advantages:

1) Z-source inverter provides the ability to boost voltage for sensorless BLDCM drive system, and then the utilization rate of dc source voltage can be improved effectively, so it is suitable for the industrial applications supplied by low-voltage dc source;
2) Z-source inverter further improves the safety of the drive system, and makes it unnecessary to consider the setting of dead-time for complementary PWM technique;
3) with the proposed approach, the sensorless BLDCM can operate within a wide speed range without switching the detection points and the reference levels, moreover, the ZCP detections are not influenced by the types of zero vectors, so it is unnecessary to change the reference levels according to the PWM technique;
4) without attenuation of the terminal voltages, the terminal voltages limited by diode can be directly compared with the reference zero level during the shoot-through vectors, so the detection error may be reduced.

## References

[1] J. Fang, W. Li, and H. Li, "Self-compensation of the commutation angle based on DC-link current for high-speed brushless DC motors with low inductance," *IEEE Trans. Power Electron.*, vol. 29, no. 1, pp. 428–439, Jan. 2014.
[2] X. Zhou and J. Fang, "Precise braking torque control for attitude control flywheel with small inductance brushless DC motor," *IEEE Trans. Power Electron.*, vol. 28, no. 11, pp. 5380–5390, Nov. 2013.
[3] Y. Liu, J. Zhao, M. Xia, and H. Luo, "Model reference adaptive control-based speed control of brushless DC motors with low-resolution hall-effect sensors," *IEEE Trans. Power Electron.*, vol. 29, no. 3, pp. 1514–1522, Mar. 2014.
[4] T. W. Chun, Q. V. Tran, H. H. Lee, and H. G. Kim, "Sensorless control of BLDC motor drive for an automotive fuel pump using a hysteresis comparator," *IEEE Trans. Power Electron.*, vol. 29, no. 3, pp. 1382–1391, Mar. 2014.
[5] J. Moreira, "Indirect sensing for rotor flux position of permanent magnet AC motors operating in a wide speed range," *IEEE Trans. Ind. Appl.*, vol. 32, no. 6, pp. 1394–1401, Nov./Dec. 1996.
[6] S. Ogasawara and H. Akagi, "An approach to position sensorless drive for brushless DC motors," *IEEE Trans. Ind. Appl.*, vol. 27, no. 3, pp. 928–933, Sep./Oct. 1991.
[7] T. Endo and F. Tajima, "Microcomputer controlled brushless motor without a shaft mounted position sensor," in *Proc. Int. Power Electron. Conf.*, 1983, pp. 1339–1345.
[8] J. Shao, D. Nolan, and T. Hopkins, "A novel direct back EMF detection for sensorless brushless DC (BLDC) motor drives," in *Proc. IEEE Appl. Power Electron. Conf.*, 2002, pp. 33–38.
[9] J. Shao, D. Nolan, M. Teissier, and D. Swanson, "A novel microcontroller-based sensorless brushless DC (BLDC) motor drive for automotive fuel pumps," *IEEE Trans. Ind. Appl.*, vol. 39, no. 6, pp. 1734–1740, Nov./Dec. 2003.
[10] Y. S. Lai, F. S. Shyu, and Y. S. Chang, "Novel sensorless PWM-controlled BLDCM drives without using position and current sensors, filter, and center-tap voltage," in *Proc. IEEE 29th Annu. Conf. Ind. Electron. Soc.*, 2003, pp. 2144–2149.
[11] Y. Kang, S. B. Lee, and J. Yoo, "A microcontroller embedded AD converter based low cost sensorless technique for brushless dc motor drives," in *Proc. 40th Ind. Appl. Conf. Annu. Meet.*, 2005, pp. 2176–2181.
[12] Y. S. Lai, F. S. Shyu, and W. H. Rao, "Novel back-EMF detection technique of brushless DC motor drives for whole duty-ratio range control," in *Proc. IEEE Annu. Conf. Ind. Electron. Soc.*, 2004, pp. 2729–2732.
[13] J. Shao, "An improved microcontroller-based sensorless brushless DC (BLDC) motor drive for automotive applications," *IEEE Trans. Ind. Appl.*, vol. 42, no. 5, pp. 1216–1221, Sep./Oct. 2006.

[14] Y. S. Lai and Y. K. Lin, "Novel back-EMF detection technique of brushless DC motor drives for wide range control without using current and position sensors," *IEEE Trans. Power Electron.*, vol. 23, no. 2, pp. 934–940, Mar. 2008.
[15] Y. S. Lai and Y. K. Lin, "A unified approach to zero-crossing point detection of back-EMF for brushless DC motor drives without current and hall sensors," *IEEE Trans. Power Electron.*, vol. 26, no. 6, pp. 1704–1713, Jun. 2011.
[16] A. Nair and K. R. Rajagopal, "A novel back-EMF detection scheme based sensorless control of permanent magnet brushless DC motor drive," in *Proc. Int. Conf. Elect. Mach. Syst.*, 2010, pp. 978–983.
[17] J. Shao, D. Nolan, and T. Hopkins, "Improved direct back EMF detection for sensorless brushless DC (BLDC) motor drives," in *Proc. IEEE Appl. Power Electron. Conf.*, 2003, pp. 300–305.
[18] F. Z. Peng, "Z-source inverter," *IEEE Trans. Ind. Appl.*, vol. 39, no. 2, pp. 504–510, Mar/Apr. 2003.
[19] F. Z. Peng, A. Joseph, J. Wang, M. Shen, L. Chen, Z. Pan, E. Ortiz-Rivera, and Y. Huang, "Z-source inverter for motor drives," *IEEE Trans. Power Electron.*, vol. 20, no. 4, pp. 857–863, Jul. 2005.
[20] S. Rajakaruna and L. Jayawickrama, "Steady-state analysis and designing impedance network of Z-source inverters," *IEEE Trans. Ind. Electron.*, vol. 57, no. 7, pp. 2483–2491, Jul. 2010.
[21] P. C. Loh, D. M. Vilathgamuwa, Y. S. Lai, G. T. Chua, and Y. W. Li, "Pulse-width modulation of Z-source inverters," *IEEE Trans. Power Electron.*, vol. 20, no. 6, pp. 1346–1355, Nov. 2005.
[22] Z. Zhou, X. Zhang, P. Xu, and W. X. Shen, "Single-phase uninterruptible power supply based on Z-source inverter," *IEEE Trans. Ind. Electron.*, vol. 55, no. 8, pp. 2997–3004, Aug. 2008.
[23] O. Ellabban, J. V. Mierlo, and P. Lataire, "A DSP-based dual-loop peak DC-link voltage control strategy of the Z-source inverter," *IEEE Trans. Power Electron.*, vol. 27, no. 9, pp. 4088–4097, Sep. 2012.
[24] G. Buja, R. Keshri, and R. Menis, "Characteristics of Z-source inverter supply for permanent magnet brushless motors," in *Proc. Ind. Electron. Conf.*, 2009, pp. 1234–1239.
[25] G. Buja, R. K. Keshri, and R. Menis, "Comparison of DBI and ZSI supply for PM brushless DC drives powered by fuel cell," in *Proc. IEEE Int. Symp. Ind. Electron.*, 2011, pp. 165–170.
[26] M. Shen and F. Z. Peng, "Operation modes and characteristics of the Z-source inverter with small inductance or low power factor," *IEEE Trans. Ind. Electron.*, vol. 55, no. 1, pp. 89–96, Jan. 2008.
[27] V. P. Galigekere and M. K. Kazimierczuk, "Analysis of PWM Z-source DC-DC converter in CCM for steady state," *IEEE Trans. Circuits Syst. I, Reg. Papers*, vol. 59, no. 4, pp. 854–863, Apr. 2012.
[28] K. Iizuka, H. Uzuhashi, M. Kano, T. Endo, and K. Morhri, "Microprocessor control for sensorless motor," *IEEE Trans. Ind. Appl.*, vol. IA-21, pp. 595–601, Aug. 1985.
[29] D. Kim, K. Lee, and B. Kwon, "Commutation torque ripple reduction in a position sensorless brushless DC motor drive," *IEEE Trans. Power Electron.*, vol. 21, no. 6, pp. 1762–1768, Nov. 2006.

**Changliang Xia** (M'08–SM'12) was born in Tianjin, China, in 1968. He received the B.S. degree from Tianjin University, Tianjin, China, in 1990, and the M.S. and Ph.D. degrees from Zhejiang University, Hangzhou, China, in 1993 and 1995, respectively, all in electrical engineering.

He is currently a Professor in the School of Electrical Engineering and Automation, Tianjin University, and also in Tianjin Key Laboratory of Advanced Technology of Electrical Engineering and Energy, Tianjin Polytechnic University. In 2008, he became "Yangtze Fund Scholar" Distinguished Professor and is currently supported by National Science Fund for Distinguished Young Scholars. His research interests include electrical machines and their control systems, power electronics, and control of wind generators.

**Xinmin Li** was born in Hunan, China, in 1989. He received the B.S. degree from the University of Science and Technology Beijing, Beijing, China, in 2011. He is currently working toward the Ph.D. degree in electrical engineering at the School of Electrical Engineering and Automation, Tianjin University, Tianjin, China.

His research interests include electrical machines and motor drives, power electronics, and wind power technology.